Manuscript Details

Manuscript number	COST_2016_287
Title	CFRP stiffened GFRP continuous beams - a simple closed-form analysis and its experimental verification for serviceability limit deformations
Article type	Full Length Article

Abstract

The small deflection analysis of equal two-span continuous simply supported GFRP beams with CFRP flange stiffening is presented for the case of equal mid-span point loads. The analysis is based on a combination of the methods of Influence Coefficients and Transformed Sections and leads to closed-form equations for tractions and deformations. Symmetric mid-span load tests on five beams – one all-GFRP and four CFRP stiffened GFRP beams – are described and mid-span deflections, support rotations are used to establish the accuracy of the analysis for predicting their deflection serviceability limits and, hence, their possible utility for the preliminary design of such beams.

Keywords	CFRP stiffeners; GFRP beams; pultrusion; serviceability limit state; shear-deformation analysis; testing

Corresponding Author	Geoffrey J. Turvey
Corresponding Author's Institution	Lancaster University
Order of Authors	Geoffrey J. Turvey

Submission Files Included in this PDF

File Name [File Type]

Cover Letter.doc [Cover Letter]

Main text rev2 - without figures & tables.doc [Manuscript File]

List of Figures and Captions.doc [Figure]

Fig 1.doc [Figure]

Fig 2.doc [Figure]

Fig 3(a).doc [Figure]

Fig 3(b).doc [Figure]

Fig 4.doc [Figure]

Fig 5.doc [Figure]

Fig 6.doc [Figure]

Fig 7.doc [Figure]

Fig 8(a).doc [Figure]

Fig 8(b).doc [Figure]

Fig 8(c).doc [Figure]

Fig 9(a).doc [Figure]

Fig 9(b).doc [Figure]

Fig 10.doc [Figure]

Fig 11(a).doc [Figure]

Fig 11(b).doc [Figure]

Fig 12(a).doc [Figure]

Fig 12(b).doc [Figure]

Fig 13(a).doc [Figure]

Fig 13(b).doc [Figure]

Fig 13(c).doc [Figure]

List of Tables and Titles.doc [Table]

Table 1.doc [Table]

Table 2.doc [Table]

Table 3.doc [Table]

Table 4.doc [Table]

To view all the submission files, including those not included in the PDF, click on the manuscript title on your EVISE Homepage, then click 'Download zip file'.

Engineering Department,
Lancaster University,
Gillow Avenue,
Bailrigg,
Lancaster,
LA1 4YW.

11th May, 2016.

Professor Antonio Ferreira,
Editor,
Composite Structures.

Dear Antonio,

CFRP stiffened GFRP continuous beams – a simple closed-form analysis and its experimental verification for serviceability limit deformations

Please would you kindly arrange for my paper, entitled as above, to be considered for publication in *Composite Structures*. It has not been submitted to any other journal for possible publication..

I look forward to receiving your decision on my paper's acceptability or otherwise for publication in due course.

Yours sincerely,

Geoff Turvey

CFRP stiffened GFRP continuous beams – a simple closed-form analysis and its experimental verification for serviceability limit deformations

by

G.J. Turvey

Engineering Department, Lancaster University, Gillow Avenue, Lancaster, LA1 4YW, UK

Abstract

The small deflection analysis of equal two-span continuous simply supported GFRP beams with CFRP flange stiffening is presented for the case of equal mid-span point loads. The analysis is based on a combination of the methods of Influence Coefficients and Transformed Sections and leads to closed-form equations for tractions and deformations. Symmetric mid-span load tests on five beams – one all-GFRP and four CFRP stiffened GFRP beams – are described and mid-span deflections, support rotations are used to establish the accuracy of the analysis for predicting their deflection serviceability limits and, hence, their possible utility for the preliminary design of such beams.

Keywords: CFRP stiffeners; GFRP beams; pultrusion; serviceability limit state; shear-deformation analysis; testing

1. Introduction

The benefits of structural continuity – especially enhanced flexural stiffness relative to single-span simply supported beams - have been exploited over many decades by the designers of continuous steel bridges and other metallic beam structures. Such benefits are of even greater significance for pultruded glass fibre reinforced polymer (GFRP) composite beam structures, which, whilst possessing many advantageous characteristics such as low self-weight, high resistance to corrosive environments etc, suffer from relatively low flexural stiffness compared to steel structures.

Various means of enhancing the flexural stiffness of pultruded GFRP beams have been investigated over the past two decades. For single-span beams, in particular, exploiting the inherent rotational stiffness of their end connections rather than simply assuming them to behave as pin joints has been investigated both analytically and experimentally (see, for example, [1] and [2]). Although a number of experimental investigations have reported rotational stiffnesses of bolted cleat connections, which are commonly used in practice (see, for example, [3] – [6] and a review of the state-of-the-art in [7]), there is, nevertheless, a reluctance amongst structural engineers to make full use of this information partly because of concerns about its reliability and the fact that the overall moment – rotation characteristics of such connections are nonlinear.

Adding higher modulus unidirectional carbon fibre reinforced polymer (CFRP) composite material to the GFRP beam to produce a hybrid fibre reinforced polymer (HFRP) beam is perhaps a more reliable means of enhancing its flexural stiffness. Two approaches have been adopted: (1) bonding (or bolting) unidirectional CFRP strip to the beam's flanges over part of its span and (2) directly pultruding an HFRP beam with CFRP rovings replacing some of the GFRP rovings in its flanges. The former approach is potentially more efficient in terms of the use of the relatively expensive CFRP material, but also involves an additional, though relatively straightforward (post pultrusion) process, namely bonding/bolting the CFRP to the beam's flanges. It is, therefore, unsurprising that the former approach to enhancing flexural stiffness has been the focus of early investigations involving single-span simply supported beams (see, for example, [8] and [9]).

Early developments and applications of single-span pultruded HFRP beams include a 610 mm deep I-section and 203 and 914 mm deep double-web custom sections (see [10] – [12]). More recently, further test and analysis investigations have been reported on single-span HFRP pultruded I-section beams in [13] and [14].

A common feature of all of the investigations cited above is that only simply supported single-span beams were considered. It appears that investigations of continuous pultruded GFRP beams are relatively few in number. In [15] equal two-span continuous beams subjected to symmetric patch loading applied at the third-span positions adjacent to the interior support were investigated. A particular focus of the investigation was the quantification of the pseudo-ductility of the GFRP bonded splice joint at that support. A subsequent investigation, reported in [16], was concerned with equal two-span pultruded GFRP wide flange (WF) continuous beams subjected to

equal mid-span point loads. Formulae, derived from first-order shear deformation analysis, were presented and shown to be useful for estimating the beam's deformations up to the serviceability deflection limit. The analysis and test work were later extended to an unequal two-span pultruded GFRP WF continuous beam with a point load applied at the centre of the longer span. New closed-form shear-rigid and shear-deformable formulae were presented and shown to provide good estimations of the serviceability limit state deformations recorded in tests (see [17] and [18]).

The present paper extends the work reported in [16] to equal two-span CFRP stiffened pultruded GFRP continuous beams subjected to equal mid-span point loads. A new exact shear deformation analysis is presented for evaluating deflections, rotations and strains when the beam is stiffened by a symmetrical arrangement of CFRP strips (of arbitrary length) bonded to the flanges at the interior support. The analysis is complemented by a series of tests on unstiffened and CFRP stiffened pultruded GFRP two-span continuous beams for which mid-span deflections, support rotations and surface strains are presented. It is shown that the test data are able to be predicted by the new analysis and it is inferred that it may usefully be used to determine the deformations of CFRP stiffened pultruded GFRP beams up to the serviceability deflection limit.

2. Shear deformation analysis of symmetrically loaded equal two-span CFRP stiffened pultruded GFRP beams

The symmetric loading and geometry of the continuous beam are shown in Fig. 1.

The length of each span is denoted by L. The ratio of the unstiffened length to the length of the span is denoted by ρ and the point load acting at the centre of each span is denoted by W. Because there is both structural and loading symmetry with respect to the interior support at C, there is no rotation at that location and, therefore, the analysis of the two-span continuous beam in Fig. 1 may be simplified to that of the propped cantilever beam shown in Fig. 2.

The CFRP stiffened pultruded GFRP propped cantilever beam shown in Fig. 2 is statically indeterminate to the first degree. It is convenient to select the reaction at B as the redundant action $R_B \left(= X \right)$. Before continuing with the analysis, the material and cross-section properties of the beam must be defined. The longitudinal elastic and transverse shear moduli of the GFRP beam are denoted by E and G, respectively. Likewise, the GFRP beam's cross-sectional area and second moment of area are denoted by A and I, respectively.
The redundant action X is determined by solving the compatibility equation at B, i.e. the downward deflection at B due to the loading alone must be equal to the upward deflection at B due to X alone, so that there is zero deflection at B. This reasoning may be expressed via the following compatibility condition,

$$X f_{11} + \mu_{10} = 0 \tag{1}$$

In Eq. (1) f_{11} is the influence coefficient for unit value of the redundant action X and μ_{10} is the load coefficient. The influence and load coefficients are determined by considering the *released* structure, i.e. the statically determinate cantilever subjected to a unit value of the redundant action and the actual loading in turn. (This method of analysis is known as the Influence Coefficient Method and further details are given in [19]). Separate bending moment and shear force diagrams have to be set up for a unit value of the redundant action and the loading on the released structure, which are then used to determine the influence coefficient f_{11} and the load coefficient μ_{10} according to Eqs. (2) and (3),

$$f_{11} = \int_0^L \frac{m_1 m_1}{EI} dL + \int_0^L \frac{s_1 s_1}{GA} dL \tag{2}$$

$$\mu_{10} = \int_0^L \frac{m_1 m_0}{EI} dL + \int_0^L \frac{s_1 s_0}{GA} dL \tag{3}$$

In Eqs. (2) and (3) m_1 and s_1 represent the bending moment and shear force distributions along the cantilever due to a unit value of the redundant action X and m_0 and s_0 denote the corresponding bending moment and shear force distributions due to the load W. dL is the incremental length of the beam. The integrals are evaluated piecewise along the length of the cantilever in Fig. 2, I and A in the denominators of Eqs. (2) and (3) are replaced with $I\left(1+\phi_I\right)$ and $A\left(1+\phi_A\right)$, respectively, where ϕ_I and ϕ_A denote the increases in the corresponding GFRP values over the the CFRP stiffened region CG in Fig. 2. It should also be appreciated that in the analysis it is assumed that $\frac{1}{2} \le \rho \le 1$, i.e. the CFRP stiffened length of the beam does not extend beyond E, the point of application of the load W.

After integrating the right hand sides of Eqs. (2) and (3), the influence and load coefficients may be expressed as,

$$f_{11} = \frac{L^3}{3EI}\left[\frac{\left(1-\rho\right)\left(1+\rho+\rho^2\right)}{\left(1+\phi_I\right)} + \rho^3 + 3\alpha\left\{\frac{\left(1-\rho\right)}{\left(1+\phi_A\right)} + \rho\right\}\right] = \frac{L^3}{3EI}\lambda_2 \tag{4}$$

and

$$\mu_{10} = \frac{WL^3}{48EI}\left[\frac{4\left(1-\rho\right)\left(1+\rho+4\rho^2\right)}{\left(1+\phi_I\right)} + \left(2\rho-1\right)^2\left(4\rho+1\right) + 24\alpha\left\{\frac{2\left(1-\rho\right)}{\left(1+\phi_A\right)} + \left(2\rho-1\right)\right\}\right] = -\frac{WL^3}{48EI}\lambda_1 \tag{5}$$

The equations for the reaction $R_B\left(=X\right)$ and the bending moments at E and C may be expressed as,

$$X = \frac{-\mu_{10}}{f_{11}} = \frac{W}{16}\frac{\lambda_1}{\lambda_2} = \frac{W}{16}\lambda \tag{6}$$

$$M_E = X\frac{L}{2} = \frac{WL}{32}\lambda \tag{7}$$

$$M_C = XL - \frac{WL}{2} = \frac{W}{16}\lambda L - \frac{WL}{2} = \frac{WL}{16}\left(\lambda - 8\right) \tag{8}$$

The deflection δ_E at E and the rotations θ_E and θ_B at E and B, respectively, are determined by applying unit forces/moments in turn at these locations and setting up the corresponding bending moment and shear force distributions, i.e. $m_{\delta_E}, s_{\delta_E}$. $m_{\theta_E}, s_{\theta_E}$ and $m_{\theta_B}, s_{\theta_B}$, which are then used in the Virtual Work (VW) equation. Thus, for example, the VW equation for δ_E becomes,

$$\delta_E = \int_0^L \frac{m m_{\delta_E}}{EI} dL + \int_0^L \frac{s s_{\delta_E}}{GA} dL \tag{9}$$

Now substituting $m = m_0 + Xm_1$ and $s = s_0 + Xs_1$ into Eq.(9) and evaluating the integrals piecewise along the beam, the formulae for the deflection at E and the rotations at E and B are determined as,

$$\delta_E = \frac{WL^3}{768EI}\left[\begin{array}{l} 4\frac{(1-\rho)}{(1+\phi_I)}\left\{16\left(1-2\rho+4\rho^2\right)-\lambda\left(1+\rho+4\rho^2\right)\right\}+\left(2\rho-1\right)^2\left\{32\left(2\rho-1\right)-\lambda\left(4\rho+1\right)\right\}+ \\ 24\alpha\left(16+\lambda\right)\left\{2\frac{(1-\rho)}{(1+\phi_A)}+\left(2\rho-1\right)\right\} \end{array}\right] \tag{10}$$

$$\theta_B = -\frac{WL^2}{32EI}\left[\frac{(1-\rho)}{(1+\phi_I)}\left\{16\rho-\left(1+\rho\right)\lambda\right\}+4\left(2\rho-1\right)^2-\lambda\rho^2\right] \tag{11}$$

$$\theta_E = -\frac{WL^2}{128EI}\left[4\frac{(1-\rho)}{(1+\phi_I)}\left\{16\rho-\left(1+\rho\right)\lambda\right\}+\left(2\rho-1\right)\left\{16\left(2\rho-1\right)-\left(2\rho+1\right)\lambda\right\}\right] \tag{12}$$

In Eqs. (4), (5) and (10) the term $\alpha\left(=\frac{EI}{GAL^2}\right)$ denotes the shear flexibility of the GFRP beam and the values of ϕ_A and ϕ_I are determined by transforming the CFRP stiffened GFRP cross-section into an equivalent all-GFRP cross-section. A GFRP beam cross-section stiffened by six CFRP strips, i.e. two strips bonded to the outer surfaces of the flanges and four narrower ones bonded to their inner surfaces, is shown in Fig. 3(a). The dimensions of the cross-section are defined in terms of the overall depth d of the GFRP section. Hence, λ_b, λ_f and λ_w denote the ratios of the width and thickness of the flange, and the thickness of the web, respectively, to the overall depth d. Likewise, α_o and α_i denote the ratios of the widths of the outer and inner CFRP strips, respectively, to the width of the flange $\lambda_b d$. Similarly, β_o and β_i denote the ratios of the outer and inner CFRP strip thicknesses, respectively, to the thickness of the flange $\lambda_f d$.

The transformed all-GFRP cross-section, equivalent to Fig. 3(a), is shown in Fig. 3(b). The shape of the cross-section is determined by increasing the widths of the CFRP strips by the factor $\gamma\left(=\frac{E_{CFRP}}{E}\right)$ where E_{CFRP} is the longitudinal elastic modulus of the CFRP. The all-GFRP transformed cross-section for the case of two CFRP strips bonded to the outer surfaces of the flanges is obtained by deleting the four rectangular domains which include the part-dashed line boundaries.

The expressions for the increase in cross-sectional area ϕ_A and second moment of area ϕ_I, corresponding to Fig. 3(b), are given in Eqs. (13) and (14), respectively,

$$\phi_A = 2\gamma\lambda_f \frac{\left(\alpha_o\beta_o+\alpha_i\beta_i\right)}{\left\{1-\left(1-\frac{\lambda_w}{\lambda_b}\right)\left(1-2\lambda_f\right)\right\}} \tag{13}$$

$$\phi_I = 2\gamma\lambda_f^3 \frac{\left[\alpha_o\beta_o^3\left\{1+3\left(1+\frac{1}{\beta_o\lambda_f}\right)^2\right\} \alpha_i\beta_i^3\left\{1+3\left(1+\frac{2}{\beta_i}-\frac{1}{\beta_i\lambda_f}\right)^2\right\}\right]}{\left[1-\left(1-\frac{\lambda_w}{\lambda_b}\right)\left(1-2\lambda_f\right)^3\right]} \tag{14}$$

Note: In Eqs. (13) and (14) the CFRP strips bonded to the outer flange surfaces have been treated as two half-strips of the same overall width as shown in Fig. 3(a).

The other deformation quantities that are of interest are the maximum strains ε_E and ε_C at E and C in Fig. 2, i.e. at the point load and the clamped support, respectively. These are evaluated as follows:-

$$\varepsilon_E = \pm\frac{M_E d}{2EI} \tag{15}$$

$$\varepsilon_C = \pm\frac{M_C d}{2EI\left(1+\phi_I\right)} \tag{16}$$

$$\varepsilon_C = \pm\frac{M_C\left(d+2t_{CFRP}\right)}{2EI\left(1+\phi_I\right)} \tag{17}$$

Eq. (16) gives the maximum strain on the outer surfaces of the GFRP beam and Eq. (17) gives the maximum strain on the outer surfaces of the CFRP strips

3. Properties of the GFRP and CFRP materials

It was decided to use EXTREN 500 series pultruded GFRP WF profiles for the continuous beam tests. The WF profiles incorporate two types of E-glass reinforcement, namely rovings (bundles of parallel fibres) and continuous filament mat (CFM). The rovings provide the beam's longitudinal stiffness and strength and the CFM provides these properties in the transverse direction. The lay-up is symmetric with a CFM layer above and below each roving layer. The outermost CFM layers are lightweight layers, which serve to create resin-rich surfaces for safe handling of the profile. The matrix material, which encapsulates and rigidises the roving and CFM layers, is an isophthalic polyester resin. The resin contains some filler material, usually kaolin or calcium carbonate, amounting to between 5 and 10% by weight. The weight percentage of glass is typically about 50%. The material used to stiffen the flanges of the GFRP WF profile is a pultruded uni-directionally reinforced CFRP strip. Its matrix material is an epoxy resin and the weight percentage of fibres is typically about 60%.

As is clear from the CFRP stiffened GFRP beam analysis in Section 2, the main material properties that need to be determined are the longitudinal elastic and shear moduli of both composite materials. A series of uniaxial tension coupon tests were carried out on rectangular, untabbed GFRP coupons and CFRP coupons with aluminium tabs to determine their longitudinal elastic moduli. No shear tests were undertaken to determine their in-plane shear moduli. Instead, it was decided to assume a value of 2.93 GPa for GFRP (based on the manufacturer's data [20]) and the same value for CFRP. Details of the tension coupon geometry and the elastic moduli determined from the tension tests on the GFRP and CFRP are given in Table1.

4. Fabrication of the CFRP stiffened continuous GFRP beams

The GFRP beam chosen for the unstiffened/stiffened continuous beam tests was a 102 x 102 x 6.4 mm (nominal dimensions) WF profile. Two beams, each 5.2 m long, were cut out of two 6 m lengths of WF profile to provide

two two-span simply supported continuous beams, each with 2.5 m spans and short overhangs (circa 50 – 100 mm) at their end supports.

Six 1 m long rectangular strips were cut out of an 80 mm wide coil of unidirectional CFRP. Four were used to provide outer surface flange stiffeners for each beam at its interior support. The other two strips were cut longitudinally to provide four 40 mm wide inner surface flange stiffeners for one of the beams.

An epoxy adhesive (Araldite 2015) was used to bond the CFRP strips to the flanges of the GFRP beams. The following procedure was used to bond a strip to the outer surface of a flange. The surface of the flange was abraded (over an area slightly greater than the contact face of the strip) to remove the resin-rich surface veil and expose the glass fibre and the abraded area was then cleaned. After removing the peel-ply from contact face of the CFRP strip, epoxy adhesive was applied to it and also to the abraded area of the flange. In order to ensure a consistent bond-line thickness 1 mm diameter transverse wire spacers were placed at 50 mm centres in the adhesive on the flange. The strip was then placed in position on the flange. Thereafter, a timber block was placed carefully on top of the strip and G-clamps were applied to hold the strip in position whilst the adhesive cured. After about one hour, adhesive spew was carefully removed from around the edges of the strip. The adhesive was left to cure and harden for a further 23 hours, after which the G-clamps were removed and the bond was visually inspected. The beam was then rotated through 180^{o} and the process was repeated to bond the other CFRP strip to the outer surface of the other flange. A similar procedure was used to bond pairs of 40 mm wide CFRP strips to the inner surfaces of the flanges, but this was not carried out until all of the tests on the beams with strips bonded to their outer flange surfaces had been completed.

The order in which the CFRP strips were bonded to the flanges of the two GFRP beams was chosen so that one unstiffened (beam U) and four CFRP strip stiffened (beams S1 – S4) GFRP continuous beams could be tested in major-axis flexure up to the serviceability deflection limit. Details of the unstiffened and CFRP strip stiffened continuous beams are given in Table 2.

5. Experimental setup and instrumentation for unstiffened/CFRP stiffened pultruded GFRP equal two-span simply supported continuous beams

Fig. 4 shows the unstiffened pultruded GFRP beam U in the test rig prior to being loaded by two equal mid-span point loads. In Fig. 5 the mid-span region of beam S1 is shown with its CFRP strip bonded to the top flange at the interior support.

A side elevation of the test setup for the CFRP stiffened GFRP beam S4 with six CFRP strips bonded to the inner and outer surfaces of its flanges is shown in Fig. 6. The strips FG, of length 1 m, were symmetrically distributed with respect to the interior support at C. The instrumentation included two 50 mm travel dial gauges with displacement resolutions of 0.01 mm in contact with the beam's soffit at the centres D and E of each span. In addition to the dial gauges, there were three electronic clinometers, which were fixed to the beam's web at mid-depth above each of the simple supports at A, B and C. Each clinometer had a high resolution (circa 0.001^{o} over the first few degrees of its range). The loads W at the centre of the top flange at D and E were applied by means of long travel hydraulic jacks with load capacities of 50 kN. The jacks shared a common connection to a hand-operated hydraulic pump, and the jack loads W were recorded by 10 kN load cells (not shown on Fig. 6). There were also pairs of uniaxial strain gauges (with 10 mm gauge lengths and their sensitive axes oriented along the span) bonded to the top and bottom surfaces of the flanges at D and E and to the top surface only at C for the unstiffened GFRP beam U. For some of the CFRP stiffened beams an additional gauge was bonded to the centre of the CFRP strip on the top flange at C. Apart from the latter gauge, all of the other gauges were inset 5 mm from the edges of the flanges in order to minimise the effects of any CFM wrinkling near those edges. The internal resistances of the strain gauges were 120 Ohms. The cross-sections shown in Figure 7 illustrate the locations and numbering of these strain gauges.

6. Test procedure and repeatability of the test data

The beam tests were carried out in the order shown in Table 2. The test procedure was similar for each beam. The loads W were applied incrementally and after each load increment the mid-span deflections and support rotations and a sub-set of the strains were recorded. This loading procedure was continued until the mid-span deflection reached approximately $1/200^{th}$ of the span (about 12.5 mm) which, for each test, was considered to be the deflection serviceability limit. (It is known that some code-like documents [21] suggest more stringent serviceability deflection limits, but it was of interest to observe whether or not linear deformation response was

maintained above these more stringent limits.). Once the deflection limit had been reached the beam was unloaded in equal decrements, again recording deflections, rotations and strains after each load decrement. Three load – unload tests were carried out on the beams. Repeat tests were necessary because the number of strain gauge channels available on the data logger was insufficient to allow all of the strain gauge readings to be recorded during a single test. This procedure enabled the repeatability of deflections and rotations to be established and all of the strain gauge readings could be recorded once. Fig. 8 shows the repeatability of the mid-span deflections for beams U, S1 and S2 for the mid-span position D. Clearly, the repeatability of the load – deflection response is good for both unstiffened and stiffened beams. Similar repeatability was obtained for the deflection at E.

The repeatability of the load – rotation response at the three simple supports is shown in Figure 9 for the beams U and S2. It is evident that the repeatability of the support rotations is excellent for the former beam but slightly less repeatable for the latter beam. Also, for the beam S2 the absolute values of the rotations measured at support B are somewhat smaller than those at A. It is also evident for both beams that the rotation at the interior support C is nominally zero and this confirms that each span is effectively functioning as an independent propped cantilever.

7. Comparison of experimental and theoretical deformations of unstiffened and CFRP stiffened GFRP beams

In order to compare the theoretical and experimental deformations of the unstiffened and CFRP stiffened equal two-span continuous beams, it is necessary to determine the various dimensionless parameters which define each beam's cross-section (cf. Fig. 3 for beam S4). The nominal cross-section of dimensions of beam S4 are shown in Figure 10.

The values of the non-dimensional parameters for each of the beams U and S1 – S4 are given in Table 3. The values of these parameters together with those for the cross-sectional area and second moment of area of the GFRP cross-section, A and I , respectively, are then used to compute the ϕ_A and ϕ_I factors given in Table 4 which account for the increases in cross-sectional area and second moment of area due to transforming the CFRP strip stiffeners into equivalent GFRP cross-section.

In addition to the values of the parameters in Tables 3 and 4, the value of the shear flexibility parameter α is also required. For beams U, S1 and S2 and beams S3 and S4 the values of α are 2.0755 x 10^{-3} and 1.88479 x 10^{-3}, respectively. The differences between the two α - values are due the fact that the longitudinal elastic modulus of the GFRP of the latter two beams is slightly smaller than that of the former three beams.

Experimental and analytical results for the mid-span deflections at point D of beams U and S2 are compared in Fig. 11(a). The experimental results for beam S1 are also presented in the same figure. However, because beam S1 is stiffened by a single CFRP strip bonded to the outer surface of its top flange, its cross-section has only one axis of symmetry, therefore the analysis presented in Section 2 is not strictly valid. Consequently, only the experimental data are presented for beam S1.

Two sets of analytical results are presented for beams U and S2. One set is for shear-deformation analysis, based on the gross area of the beams' cross-section A_g , and the other for the classical shear-rigid (S-R) analysis. It is evident that the load – deflection response for the unstiffened beam U is predicted very well by the shear-deformation analysis, whereas the classical S-R analysis is significantly over-stiff. Indeed, it provides a reasonable prediction for beam S1's load – deflection response. However, both analyses over-predict the flexural stiffness of beam S2 with the shear-deformation analysis providing the smaller over-prediction. A similar set of load – deflection comparisons were obtained for the mid-span points E of the beams.

Load – deflection comparisons for the mid-span point D of beams S3 and S4 are shown in Fig. 11(b). In this case, it is evident that the shear-deformation analysis predicts the experimental response of beam S3 very well and that of beam S4 quite well. Somewhat surprisingly, the S-R analysis of beam S3 predicts the experimental response of beam S4 with about the same degree of accuracy as the shear-deformation analysis of beam S4. Again, the S-R analysis of beam S4 is significantly stiffer than the experimental response. Similar response comparisons were obtained for the other mid-span points E.

Experimental and analytical load – rotation response comparisons for support A are presented for beams U, S1 and S2 and beams S3 and S4 in Figures 12(a) and 12(b), respectively. Fig. 12(a) shows that the shear-

deformation analysis based on the web cross-sectional area A_w provides a more accurate simulation of beam U's response than the corresponding analysis based on the gross cross-sectional area A_g . Indeed, the latter analysis simulates beam S1's response very accurately. As for beam S2, both shear- deformation analyses provide over-stiff predictions of its load – rotation response at A with the analysis based on the web cross-sectional area being somewhat less over-stiff. Similar comparisons, with the rotations being equal but of opposite sign, were obtained for support B. However, in Fig. 12(b) it is evident that the shear-deformation analyses for beams S3 and S4 are only very slightly over-stiff compared to the experimental load – rotation responses.

The theoretical outer surface flange strains have been computed using Eqs. (15) – (17) and are compared with the corresponding averaged strains in Fig. 13 for beams U, S2 and S4.

It is evident in Fig. 13(a) for beam U that the average strains on the top flange (TF) and bottom flange (BF) at the mid-span points D and E are in good agreement. As expected, the average experimental strain on the top flange at the interior support is somewhat larger than the bottom flange average strains at D and E. However, the theoretical BF and TF average strains at the mid-span points D and E are over-estimated by the shear-deformation analysis. In fact the BF average strains provide excellent predictions of the higher TF average strains at the interior support C.

Figure 13(b) shows similar sets of BF and TF average strains for beam S2. It is evident that there is closer agreement between the BF average strains at the mid-span points D and E than between the TF strains. Again, the BF and TF strains at the centre of each span are over-estimated by the shear-deformation analysis. Likewise, the TF average experimental strains at C, recorded on the GFRP material are over-estimated by theory (Th), but the strains recorded on the surface of the CFRP stiffener are in very good agreement with the theoretical values.

The correlations between the measured and predicted strains for beam S4 are shown in Fig. 13(c). It is noticeable that the TF and BF average strains at the mid-span points D and E are consistent and repeatable. However, the theoretical strains over-predict the measured strains at these points. The TF average strains recorded at C are greater than the BF strains at the mid-span points D and E.

8. Concluding remarks

Based on the Method of Influence Coefficients and the concept of Transformed Sections for multi-material beam cross-sections, closed-form equations have been presented for predicting the serviceability deformation response of equal two-span continuous pultruded GFRP beams with CFRP flange stiffening at the interior support when subjected to equal mid-span point loads.

Five beams – one unstiffened and four with three CFRP stiffening arrangements have been tested up to the deflection serviceability limit of $1/200^{th}$ of the span. During the tests mid-span deflections, support rotations and surface strains at the mid-spans and the interior support were recorded to provide data for the verification of the closed-form analysis.

Repeat testing of each beam configuration demonstrated that the mid-span deflections and support rotations were both linear and repeatable up the deflection serviceability limit.

Comparison of the mid-span deflection data for the unstiffened and CFRP stiffened pultruded GFRP continuous beams revealed that the theoretical analysis tended to predict the unstiffened response accurately and to slightly under-predict the CFRP stiffened beam response up to the serviceability deflection limit. These observations suggest that the closed-form analysis could be used for preliminary design for the deflection serviceability limit state, as a range of CFRP stiffener lengths and layouts could be rapidly assessed.

Finally, the experimental/theoretical results comparisons vindicate the use of the combination of the Influence Coefficient Method and Transformed Sections as a viable and simple means of analysing hybrid fibre (CFRP/GFRP) beams for the serviceability deformation response.

9. Acknowledgements

The Author wishes to express his appreciation to Messrs J. Merlet and J-P. Campredon, who, under the Author's supervision, contributed to the test work during their Summer Internships in the Engineering Department. In

addition, he wishes to thank Mr. M. Salisbury of the Engineering Department's Technician Staff, who also contributed to the test work. Finally, the Author wishes to acknowledge his appreciation to The Engineering Department for providing the use of its Structures and Materials Testing Laboratories, without which this work could not have been completed.

References

1. Turvey GJ. Analysis of pultruded glass reinforced plastic beams with semi-rigid end connections. Composite Structures 1997; 38(1-4): 3-16.
2. Turvey GJ. Flexure of pultruded GRP beams with semi-rigid end connections. Composite Structures 1999; 47(1): 571-80.
3. Turvey GJ, Cooper C. Semi-rigid pultruded GRP frame connections: tests to determine static moment-rotation characteristics. In ECCM-7 (seventh european conference on composite materials: realising their commercial potential), Vol.2, Woodhead Publishing Limited, Cambridge, 1996, 295-300.
4. Turvey GJ. Moment – rotation tests on bolted end connections in pultruded GRP beams – tests with stainless steel cleats. Proceedings of ECCM 9 (composites – from fundamentals to exploitation), Brighton, 4 – 7 June 2000 [CD Rom Proceedings].
5. Quereshi J and Mottram JT. Response of beam-to-column web-cleated joints for FRP pultruded members. Journal of Composites for Construction 2014; 18(2):
6. Qureshi J, Mottram JT. Behaviour of pultruded beam-to-column joints using steel web cleats. Thin-Walled Structures 2013; 73:48-56
7. Turvey GJ, Cooper C. Review of tests on bolted joints between pultruded GRP profiles. Proceedings of the Institution of Civil Engineers: Structures & Buildings 2004; 157(3):211-33.
8. Turvey GJ. Structural analysis of CFRP-plated pultruded GRP beams. Proceedings of the Institution of Civil Engineers: Structures & Buildings 2006; 159(SB2):65-75.
9. Turvey GJ. Analysis of bending tests on CFRP-stiffened pultruded GRP beam. Proceedings of the Institution of Civil Engineers: Structures & Buildings 2007; 160(SB1): 37-49.
10. Anon. First hybrid I-girder bridge. FRP International 1997; 5(1):4.
11. Witcher DA. Development and production of heavy structural FRP composites for use a priary structural components. Proceedings of the second international conference on composites in infrastructure (ICCI 98), Tucson, 5 – 7 January 1998, Vol. II, 327-40.
12. Hayes MD, Waldron C, Schniepp T, Lesko JJ and Cousins TC. Implementation of the deep DWB in the Dickey Creek bridge. Proceedings of the international SAMPE symposium and exhibition, 2001 46 II pp.1587-96.
13. Hai ND, Mutsuyoshi H, Asamoto S, Matsui T. Structural behaviour of hybrid FRP composite I-beams. Construction and Building Materials 2010; 24(6):956-69.
14. Mutsuyoshi H, Hai ND, Shiroki K, Aravinthan T, Manalo A. Experimental investigation of HFRP composite beams. American Concrete Institute, Special Publication 1 (275SP) pp.219-243, 2011.
15. Keller T, de Castro J. System redundancy and ductility of FRP beam structures with ductile adhesive joints. Composites Part B: Engineering 2005; 36(8):586-96.
16. Turvey G. Pultruded GFRP continuous beams – comparison of flexural test data with analysis predictions. Advanced composites in construction conference 2011(ACIC 2011), 6th – 8th September 2011, University of Warwick, 470-481.
17. Turvey GJ. Bending of unequal span continuous pultruded glass fibre reinforced polymer (GFRP) beams. Proceedings of the 7th International Conference on Advanced Composites in Construction, 9th – 11th September 2015, University of Cambridge, UK (CD Rom Proceedings).
18. Turvey GJ. Testing and analysis of pultruded GFRP continuous beams for the deflection serviceability limit state. Composite Structures 2016; 141( ):213-20.
19. Morice PB. Linear structural analysis: an introduction to the influence coefficient method applied to statically indeterminate structures. London: Thames and Hudson; 1969.
20. Anon., EXTREN fiberglass structural shapes: design guide. Bristol VA: 1989.
21. Clarke JA (ed). EUROCOMP design guide. London: E & FN Spon: 1996.

List of figures and captions

Fig 1.doc

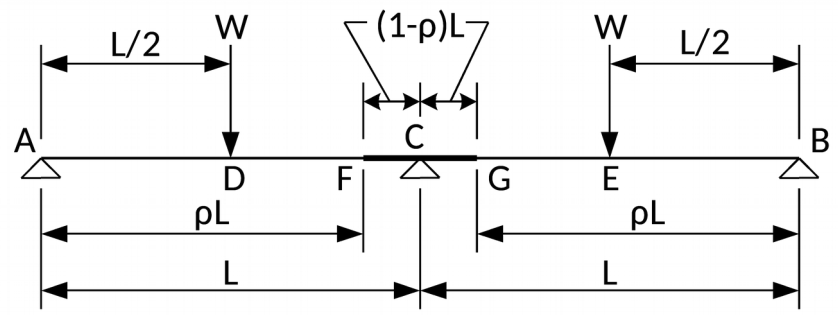

Fig. 1

Fig 2.doc

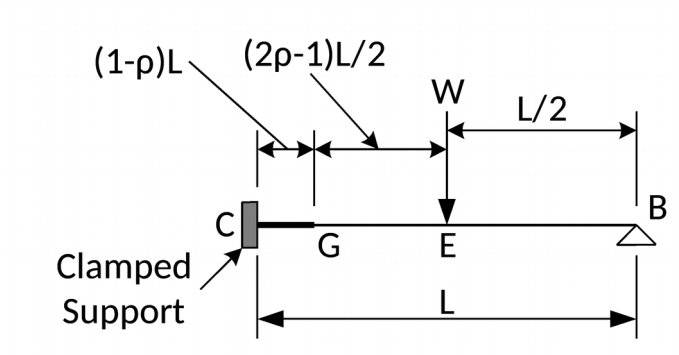

Fig. 2

Fig 3.doc

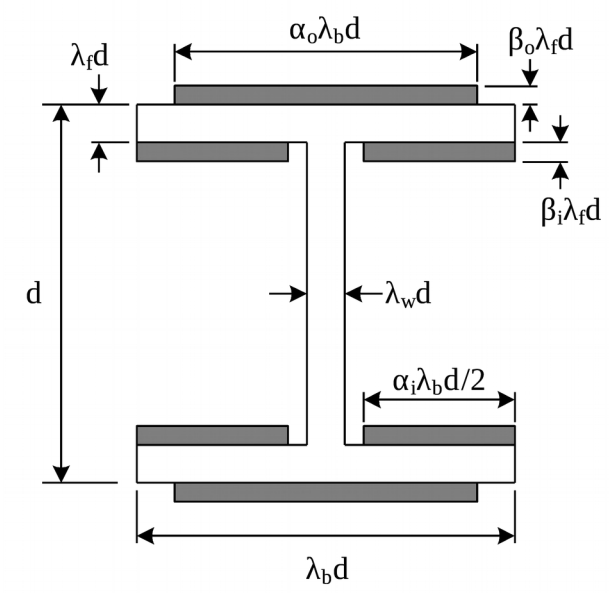

Fig. 3(a)

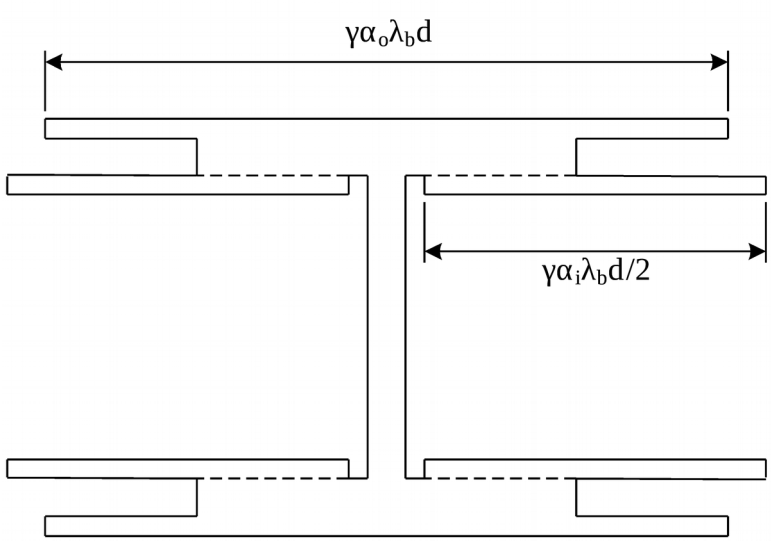

Fig. 3(b)

Fig 4.doc

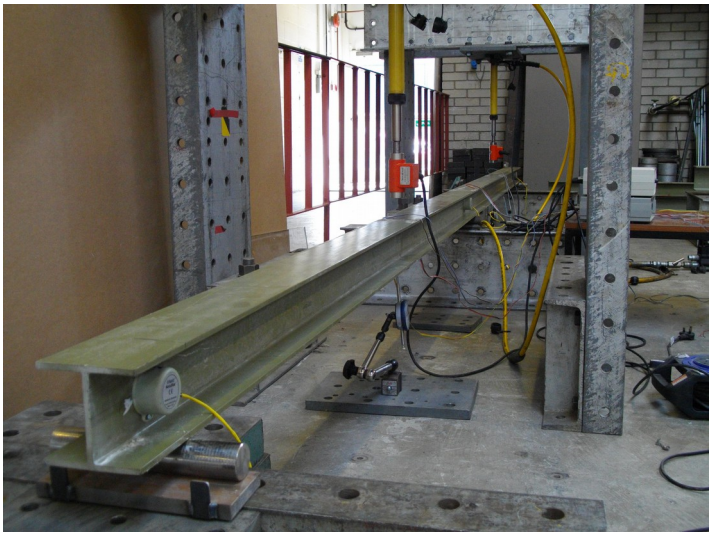

Fig. 4

Fig 5.doc

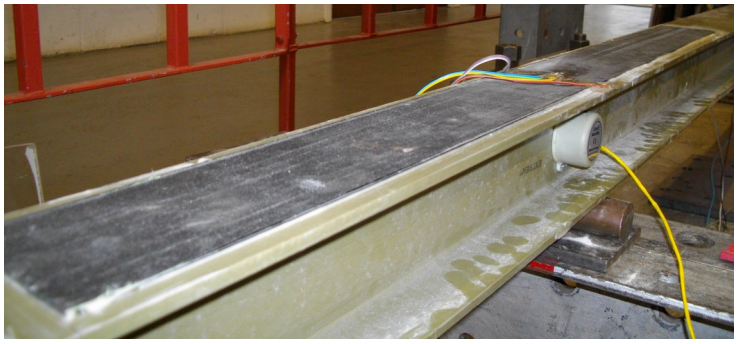

Fig. 5

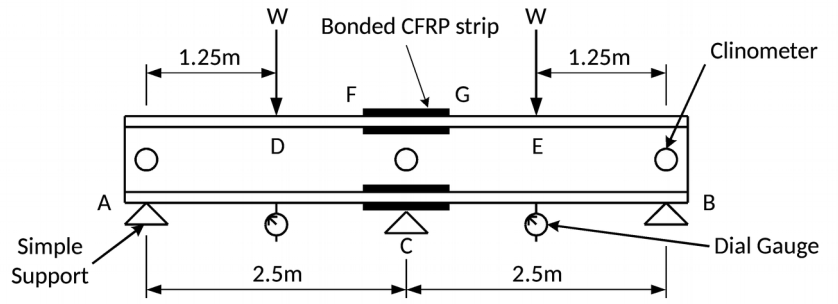
W
Bonded CFRP strip
W
1.25m
1.25m
Clinometer
F
G
D
E
A
B
Simple
Support
C
Dial Gauge
2.5m
2.5m

Fig. 6

Fig 7.doc

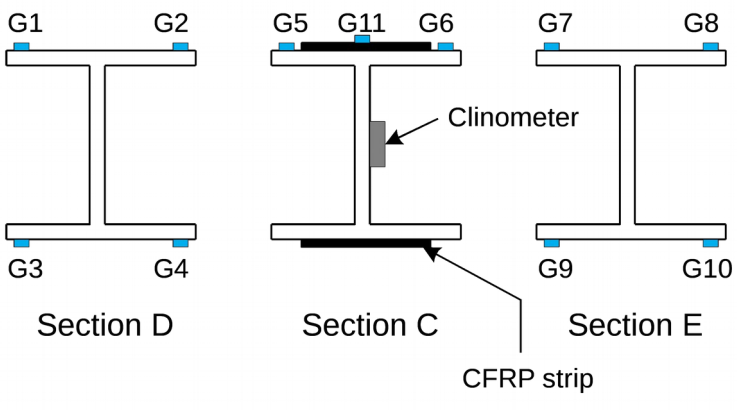

Fig. 7

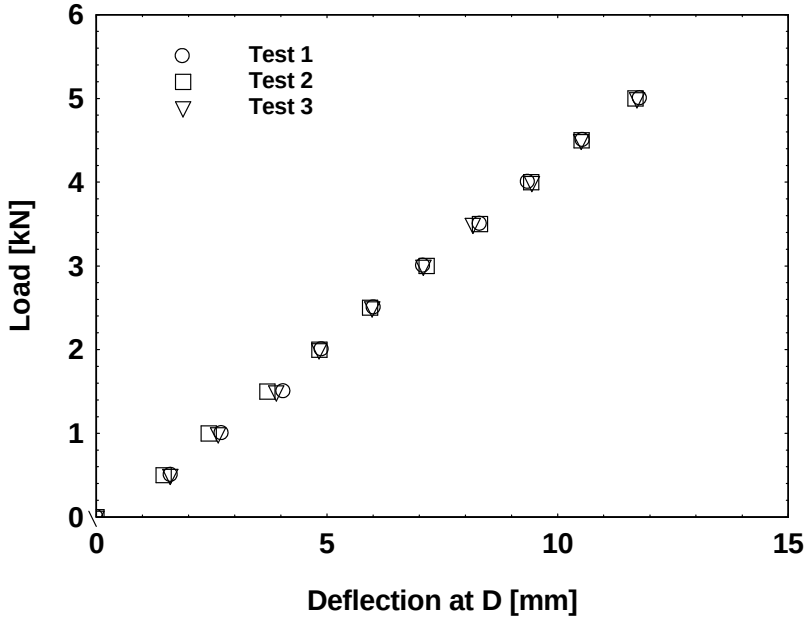

Fig. 8(a)

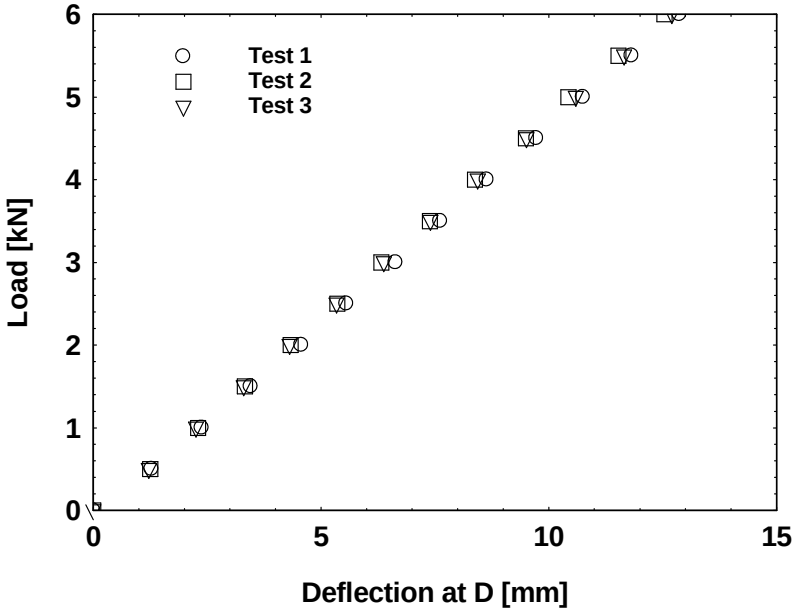

Fig. 8(b)

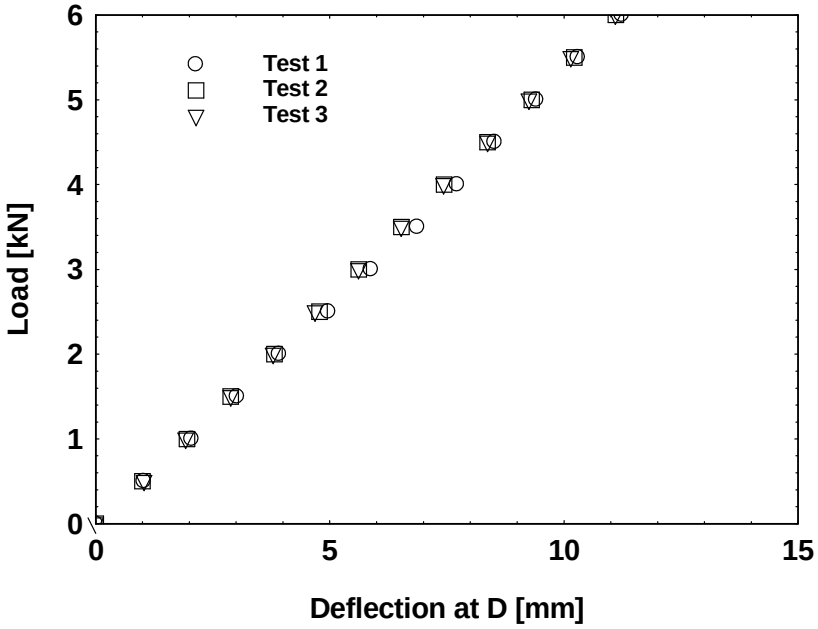

Fig. 8(c)

Fig 9(a).doc

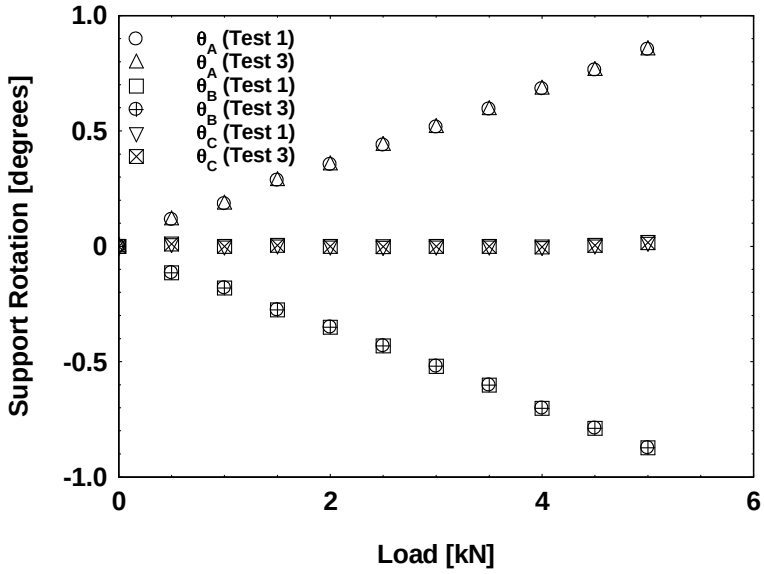

Fig. 9(a)

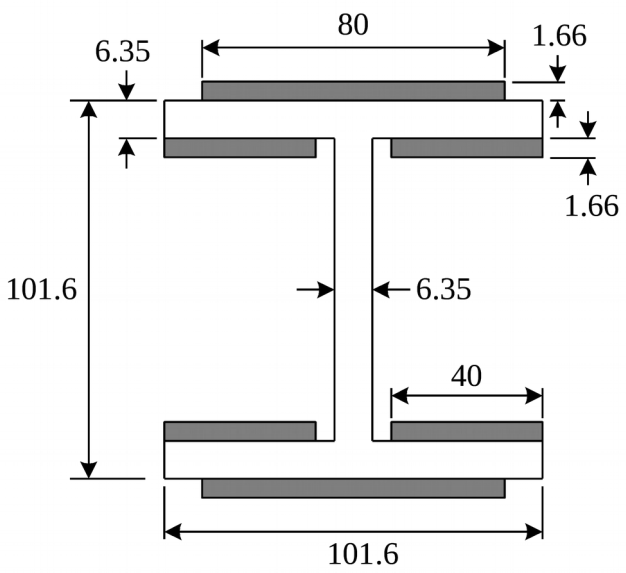

Fig. 10

Fig 9(b).doc

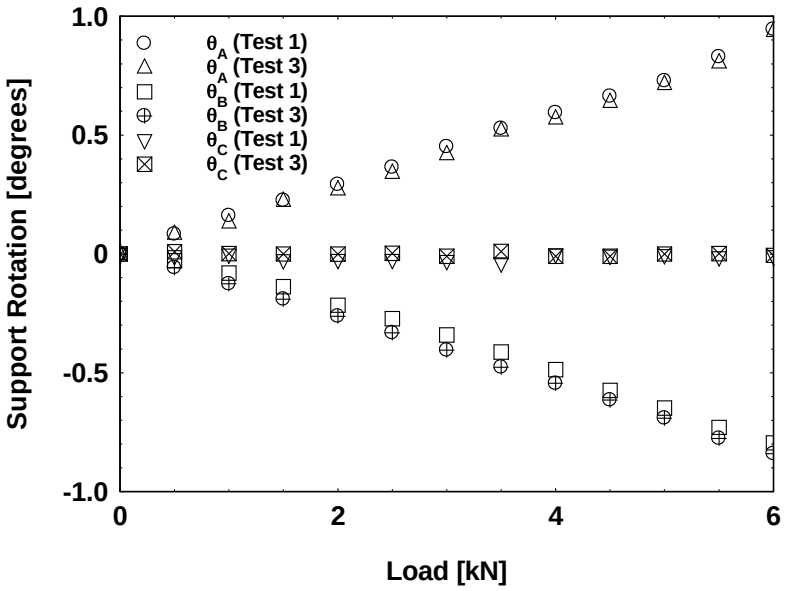

Fig. 9(b)

Fig 11(b).doc

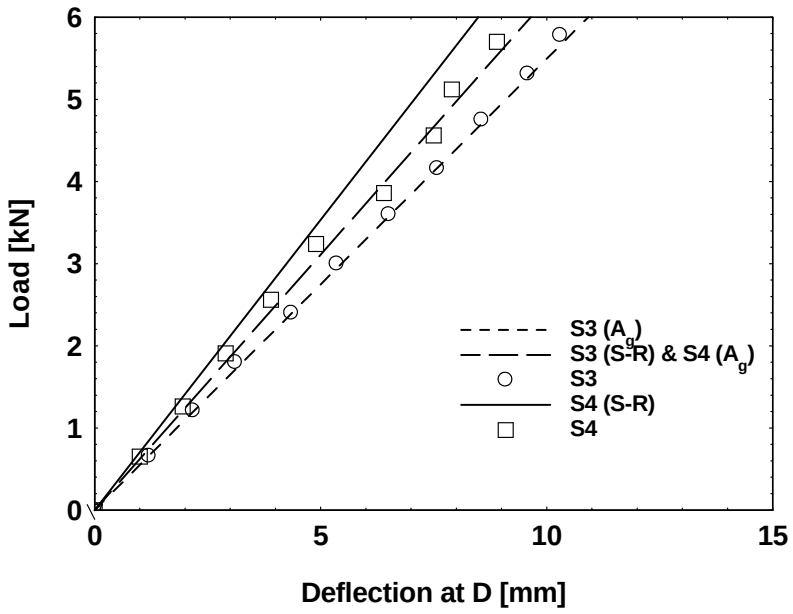

Fig. 11(b)

Fig 11(a)

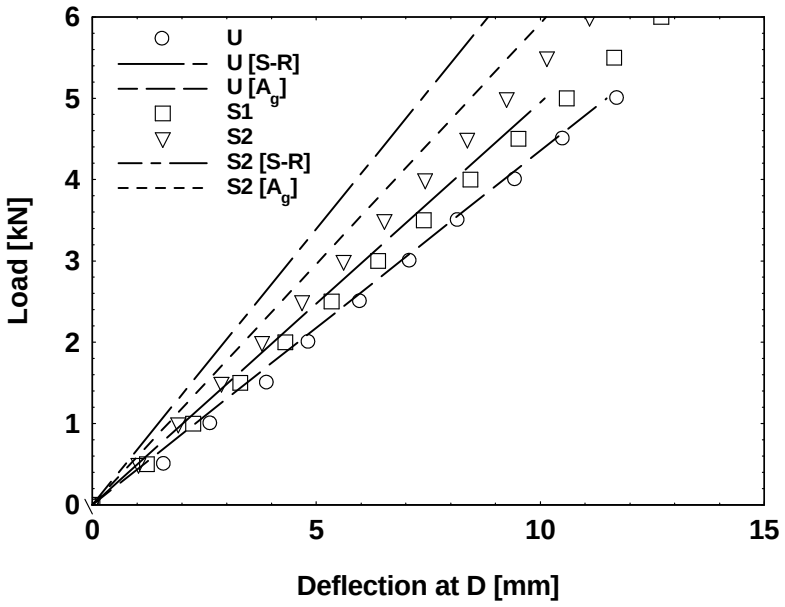

Fig. 11(a)

Fig 12(b).doc

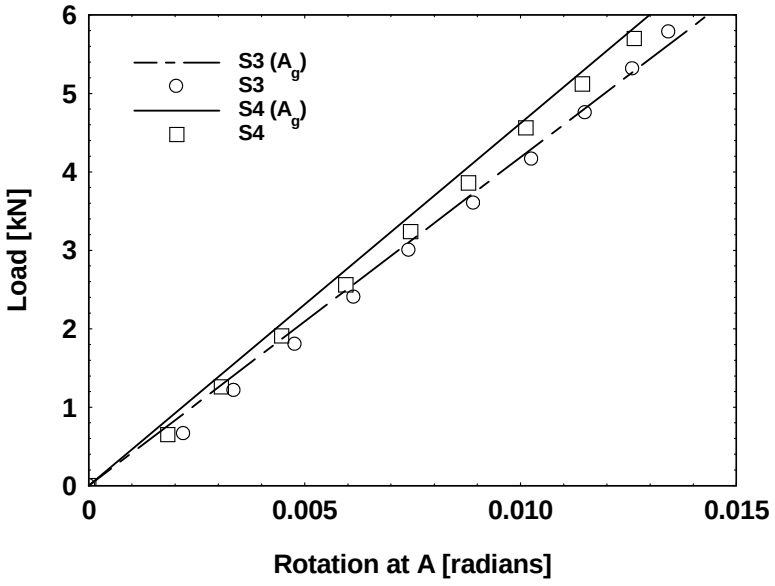

Fig. 12(b)

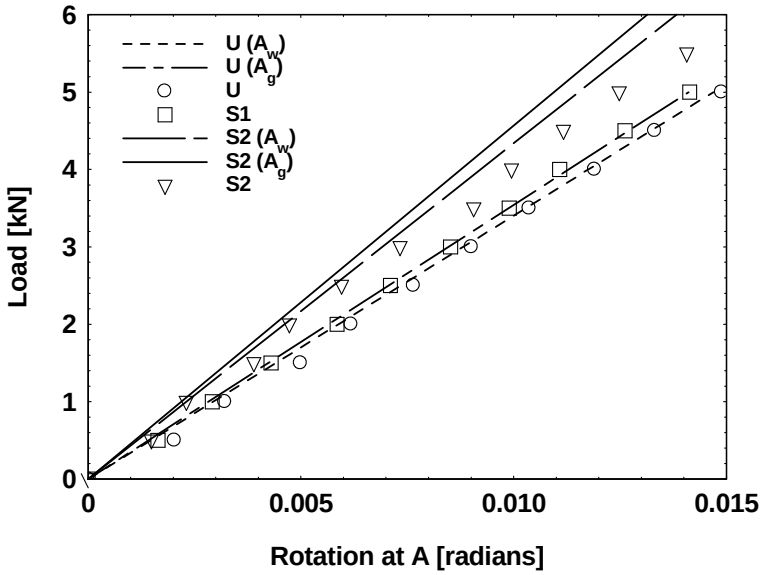
U (A_w)
U (A_g)
U
S1
S2 (A_w)
S2 (A_g)
S2
Load [kN]
Rotation at A [radians]
0
1
2
3
4
5
6
0
0.005
0.010
0.015

Fig. 12(a)

Fig 13(b).doc

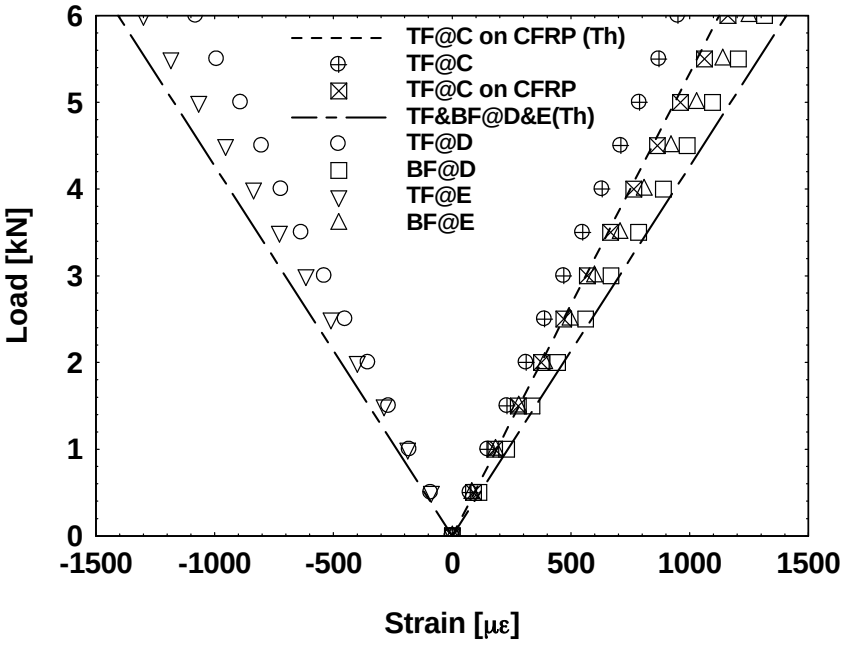

Fig. 13(b)

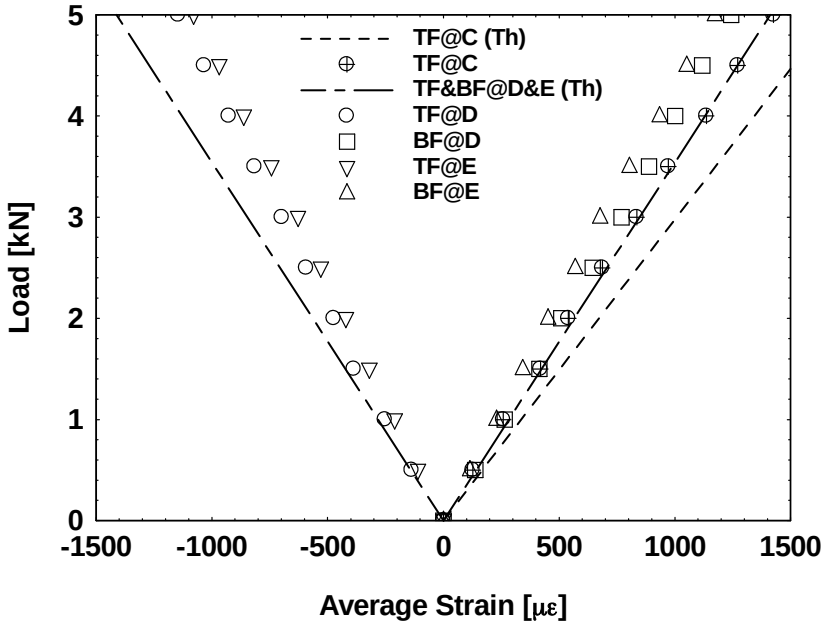
TF@C (Th)
TF@C
TF&BF@D&E (Th)
TF@D
BF@D
TF@E
BF@E
Load [kN]
Average Strain [με]
5
4
3
2
1
0
-1500
-1000
-500
0
500
1000
1500

Fig. 13(a)

List of Tables and Titles

Fig 13(c).doc

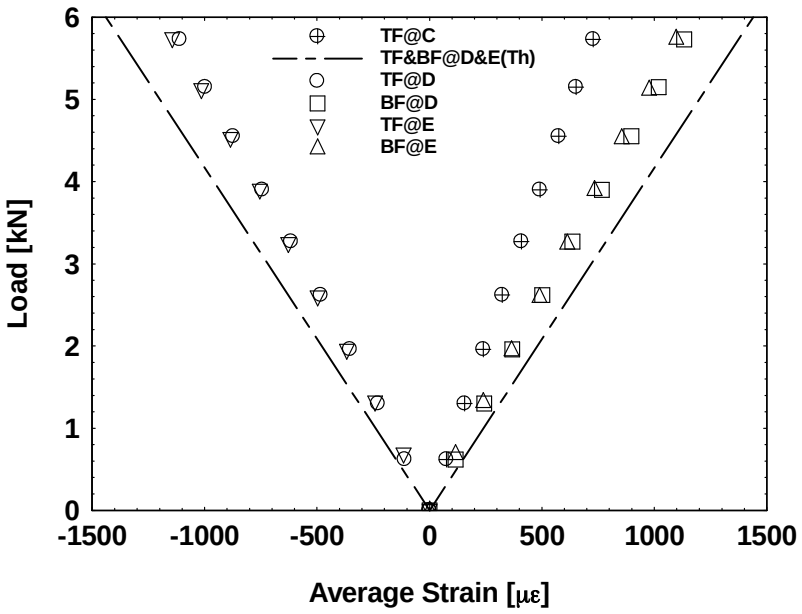

Fig. 13(c)

Table 2

Details of the unstiffened and CFRP stiffened GFRP continuous beams

Beam Designations	**Number of CFRP strips on flange surfaces (outer/inner)**	**CFRP strip widths (outer/inner)** **[mm]**	**CFRP strips (length/thickness)** **[mm]**	**Span lengths (span 1/span 2)** **[m]**
U	0/0	0	0/0	2.5/2.5
S1	1/0	80/0	1000/1.66	
S2	2/0	80/0	1000/1.66	
S3	2/0	80/0	1000/1.66	
S4	2/4	80/40	1000/1.66	

Table 1

Tension coupon geometry and elastic moduli of the GFRP beam and the CFRP strip material [Coupon length = 300 mm and grip length = 50 mm]

Material	**Test number**	**Mean width [mm]**	**Mean thickness [mm]**	**Mean cross-sectional area [mm^2]**	**Longitudinal elastic modulus [GPa]**
GFRP	1	24.22	6.69	162.1	22.24
	2	24.46	6.70	163.9	21.16
	3	24.59	6.57	161.6	20.62
	4	24.84	6.61	164.2	21.43
CFRP	1	25.11	1.66	41.18	133.1
	2	25.20	1.66	41.33	137.4

Notes: (1) The GFRP coupons were cut longitudinally out of the beam's flanges.
(2) These properties were obtained for beams U, S1 and S2. Slightly lower longitudinal elastic modulus values were determined for beams S3 and S4 (see Section 7).

Table 4

Cross-sectional area and major-axis second moment of area of the GFRP beams and the ϕ-factors defining the increases in these quantities arising from transforming the CFRP strips to equivalent GFRP material

Beam	$A\left(=A_g\right)$ [x 10^3 mm^2]	$I\left(=I_g\right)$ [x 10^6 mm^4]	ϕ_A	ϕ_I
U	1.8548	3.3028	0.0	0.0
S1			*	*
S2			0.9068	1.3576
S3			0.9068	1.3576
S4			1.8945	2.4305

Note: * denotes that the values were not determined because Eqs. (13) and (14) do not apply

Table 3

Dimensionless parameters which define the beams' transformed cross-sections

Beam	λ_b	λ_f	λ_w	α_o	α_i	β_o	β_i	γ
U	1.0	0.0625	0.0625	0.0	0.0	0.0	0.0	1.0
S1				0.7874	0.0	0.2614	0.0	6.3325
S2				0.7874	0.0	0.2614	0.0	6.3325
S3				0.7874	0.0	0.2614	0.0	6.6153
S4				0.7874	0.7874	0.2614	0.2614	6.6153

Note: $d = 101.6\ mm$